Electronic Supplementary Information For

Ferroelectricity and Antiferromagnetism in Organic–inorganic Hybrid (1,4-Bis(imidazol-1-ylmethyl)benzene)$CuCl_4 \cdot H_2O$

Chunli Jiang,[a] Qianqian Luo,[b] Hanmei Fu,[b] Hechun Lin,[b] Chunhua Luo,[b] Jianlu Wang,*[a] Xiangjian Meng,[a], Hui Peng,*[b][c] Chun-Gang Duan,[b][c] and Junhao Chu[a]

[a] National Laboratory for Infrared Physics, Shanghai Institute of Technical Physics, Chinese Academy of Science, Shanghai 200083, China.

[b] Key Laboratory of Polar Materials and Devices (MOE), Department of Electronics, East China Normal University, Shanghai, 200241, China.

[c] Collaborative Innovation Center of Extreme Optics, Shanxi University, Taiyuan, Shanxi.

Crystallographic Data

Table S1. Crystal data and structure refinement for (bix)$CuCl_4 \cdot H_2O$.

Compound	(bix)$CuCl_4 \cdot H_2O$
Chemical formula	$C_{14}H_{18}Cl_4CuN_4O$
Formula weight	461.65
Temperature /K	173
Crystal system	monoclinic
Space group	*P*c
a /Å	7.1235(2)
b /Å	11.1935(4)
c /Å	11.6744(4)
α /°	90
β /°	97.716(1)
γ /°	90
V /Å^3	922.45(5)
Z	2
ρ_{calc}g /cm^3	1.669
μ /mm^{-1}	7.089
F(000)	470.0
h, k, l_{max}	8,13,14
θ_{max}	68.185
R_1[I>2σ I][a]	0.0268
wR2	0.0678
S	1.121

Table S2. Selected bond lengths (Å) and bond angles (°) for (bix)$CuCl_4 \cdot H_2O$

Cu1−Cl1	2.2483(8)	Cl2−Cu1−Cl1	131.96(4)
Cu1−Cl2	2.2738(9)	Cl2−Cu1−Cl3	97.95(4)
Cu1−Cl3	2.2320(9)	Cl3−Cu1−Cl1	99.01(3)
Cu1−Cl4	2.2489(10)	Cl4−Cu1−Cl1	101.18(4)
		Cl4−Cu1−Cl2	96.77(3)
		Cl4−Cu1−Cl3	136.14(4)

Table S3. Hydrogen bonds of compound (bix)$CuCl_4 \cdot H_2O$

D−H···A	d(D−H) (Å)	d(H···A) (Å)	d(D···A) (Å)	∠(DHA) (°)
N(4)−H(4)···Cl(2)	0.88	2.31	3.110(3)	151
N(2)−H(2)···O(1)	0.88	1.89	2.748(5)	164
O(1)−H(1B)···Cl(3)	0.85	2.43	3.173(4)	147
O(1)−H(1A)···Cl(4)	0.84	2.44	3.253(4)	162

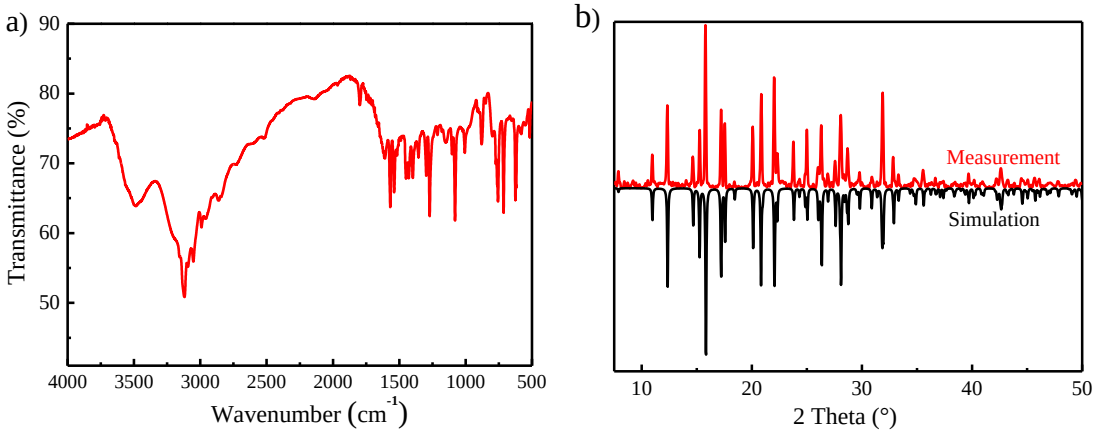

Fig. S1. (a) Infrared spectrum and (b) powder XRD patterns of (bix)$CuCl_4 \cdot H_2O$, verifying the purity of the bulk phase.

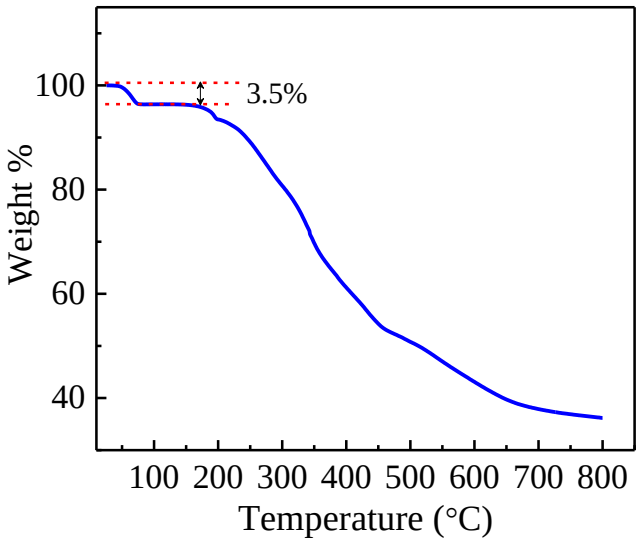

Fig. S2. TGA curve of (bix)$CuCl_4 \cdot H_2O$.

Fig. S3. Images for powder of the as synthesized and dehydrated phase of (bix)$CuCl_4 \cdot H_2O$.

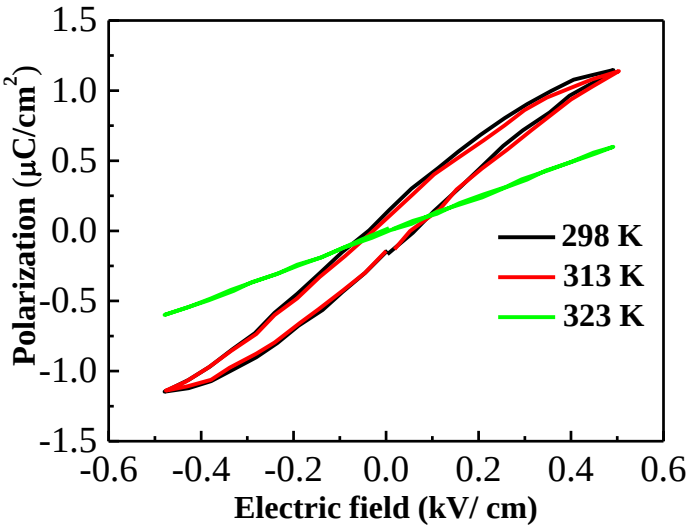

Fig. S4. *P-E* hysteresis loops recorded on crystal of (bix)$CuCl_4 \cdot H_2O$ at different temperatures with frequency of 50 Hz.

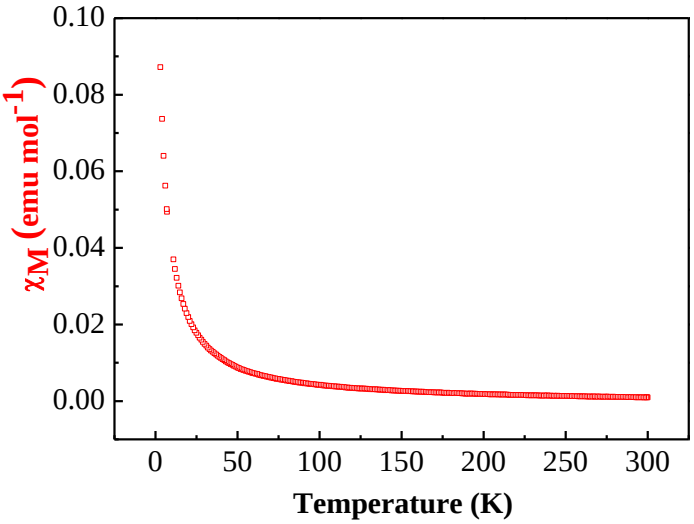

Fig. S5. Temperature dependence of the molar magnetic susceptibility (χM) for the dehydrated sample.

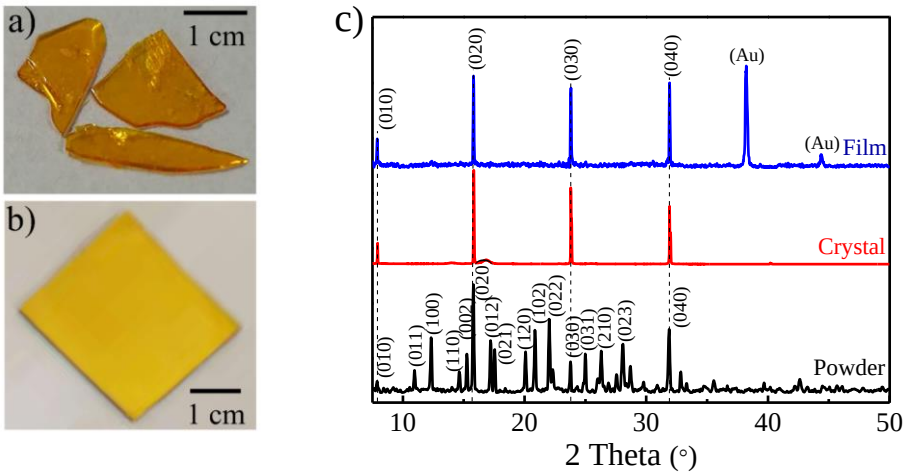

Fig. S6. Optical photographs of crystals (a), thin film of (bix)$CuCl_4 \cdot H_2O$ on Au/glass substrate (b) and their XRD patterns compared with the powder sample (c).

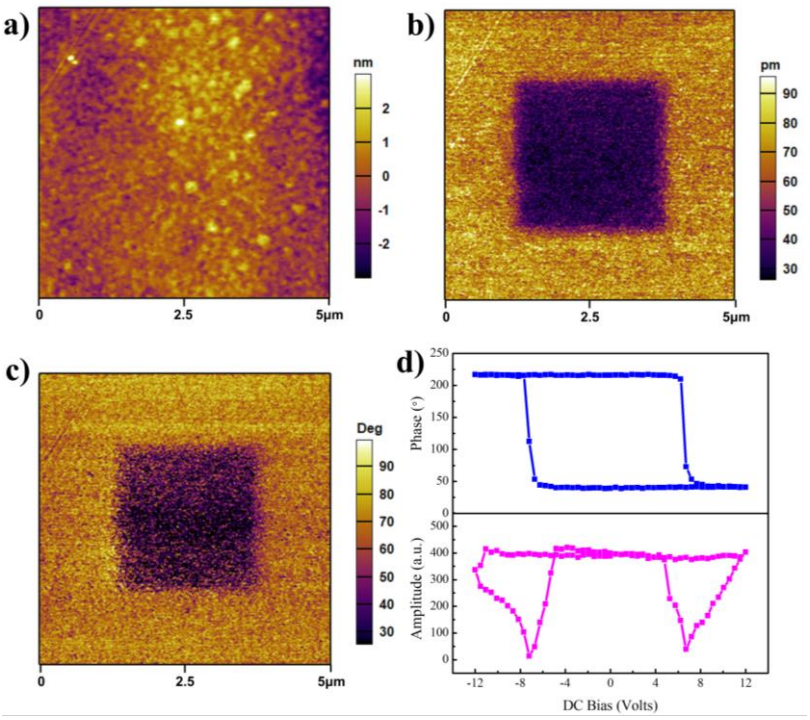

Fig. S7. PFM images and polarization switching for the thin film of (bix)$CuCl_4 \cdot H_2O$. (a) Topographic image, (b) amplitude image and (c) phase image recorded after applying -9 V and +9 V voltage. (d) Hysteresis and butterfly loops.